

PCCP

Accepted Manuscript



This is an *Accepted Manuscript*, which has been through the Royal Society of Chemistry peer review process and has been accepted for publication.

Accepted Manuscripts are published online shortly after acceptance, before technical editing, formatting and proof reading. Using this free service, authors can make their results available to the community, in citable form, before we publish the edited article. We will replace this *Accepted Manuscript* with the edited and formatted *Advance Article* as soon as it is available.

You can find more information about *Accepted Manuscripts* in the [Information for Authors](#).

Please note that technical editing may introduce minor changes to the text and/or graphics, which may alter content. The journal's standard [Terms & Conditions](#) and the [Ethical guidelines](#) still apply. In no event shall the Royal Society of Chemistry be held responsible for any errors or omissions in this *Accepted Manuscript* or any consequences arising from the use of any information it contains.

Controlled Direct Growth of Al₂O₃-doped HfO₂ Films on Graphene by H₂O-based Atomic Layer Deposition

Cite this: DOI: 10.1039/x0xx00000x

Li Zheng,^a Xinhong Cheng,^{*a} Yuehui Yu,^a Yahong Xie,^b Xiaolong Li^c and Zhongjian Wang^a

Received 00th January 2012,

Accepted 00th January 2012

DOI: 10.1039/x0xx00000x

www.rsc.org/

Graphene has been drawing worldwide attention since its discovery in 2004. In order to realize graphene-based devices, thin, uniform-coverage and pinhole-free dielectric films with high permittivity on top of graphene are required. Here we report the direct growth of Al₂O₃-doped HfO₂ films onto graphene by H₂O-based atomic layer deposition (ALD). Al₂O₃-onto-HfO₂ stacks benefited the doping of Al₂O₃ into HfO₂ matrixes more than HfO₂-onto-Al₂O₃ stacks did due to the micro-molecular property of Al₂O₃ and high chemical activity of trimethylaluminum (TMA). Al₂O₃ acted as a network modifier, maintained the amorphous structure of the film even to 800 °C, and made the film smooth with the root mean square (RMS) roughness of 0.8 nm, comparable to the surface of pristine graphene. The capacitance and the relative permittivity of Al₂O₃-onto-HfO₂ stacks were up to 1.18 μF/cm² and 12, respectively, indicating high quality of Al₂O₃-doped HfO₂ films on graphene. Moreover, the growth process of Al₂O₃-doped HfO₂ films introduced no detectable defects into graphene confirmed by Raman measurements.

1. Introduction

Graphene, a fascinating two-dimensional (2D) material, has shown promise as a silicon replacement since its discovery in 2004.¹ It possesses extraordinary properties such as high room temperature mobility (200,000 cm²V⁻¹s⁻¹),² unconventional noninteger quantum-Hall effect,³ and tunable band gaps in nanostructures carved from it.⁴ In order to fabricate graphene-based electronic devices, ultra-thin high-κ dielectrics should be prepared on graphene.⁵⁻⁹ In recent years, ALD was emerged as a powerful method for controlled deposition of ultra-thin and uniform dielectric films.¹⁰⁻¹⁴ Unfortunately, the chemical inertness of graphene makes it challenging to nucleate and grow a uniform thin layer of high-κ dielectrics directly by ALD. Functionalization of graphene surface and a transition layer (a thin oxidized metal layer or a polymer buffer layer) have been developed to form gate insulators by ALD.¹⁵⁻¹⁷ However, functionalization leads to degradation of graphene mobility while a transition layer increases the equivalent oxide thickness (EOT) of dielectric films. In our previous work, we tried to deposit Al₂O₃ and HfO₂ films directly onto graphene by H₂O-based ALD.¹⁸⁻²⁰ Al₂O₃ is known to remain in amorphous state even upon heating to temperatures as high as 800 °C. However, its relative permittivity (7-9) is relatively small, which leads to a high EOT. Although the relative permittivity of amorphous HfO₂ can be as high as 15-25, it is prone to crystallization upon heating with the associated decrease in relative permittivity.^{21,22} Therefore, how to deposit a dielectric film with both high relative permittivity and thermal stability is an urgent issue to be addressed. Here we report a direct ALD growing process of

Al₂O₃-doped HfO₂ films onto graphene. Physically adsorbed H₂O on graphene surface has been shown to serve as an effective surfactant allowing for an ultra-thin layer of HfO₂ covering graphene surface. The Al₂O₃-doped HfO₂ (Al₂O₃-onto-HfO₂ stacks) film was achieved by two-temperature (100/200 °C) deposition of Al₂O₃ over HfO₂ film. Al₂O₃-onto-HfO₂ stacks benefited the doping of Al₂O₃ into HfO₂ matrixes more than HfO₂-onto-Al₂O₃ stacks did. The Al₂O₃-onto-HfO₂ stacks were observed to remain in amorphous state for temperatures as high as 800 °C. Raman spectra were performed to indicate whether H₂O-based ALD introduced defects or disorder into graphene. X-ray photoelectron spectroscopy (XPS) was implemented to confirm the element components in Al₂O₃-onto-HfO₂ stacks on graphene. Atomic force microscope (AFM) and high resolution transmission electron microscopy (HRTEM) were carried out to show the surface morphology and microstructure of Al₂O₃-onto-HfO₂ stacks film on graphene, respectively. Grazing incidence X-ray diffraction (GIXRD) was employed to confirm the amorphous state of the Al₂O₃-HfO₂ layer stacks. In addition, spectroscopic ellipsometer (SE) and capacitance-voltage (C-V) measurements were also utilized to reveal the high quality of Al₂O₃-onto-HfO₂ stacks on graphene. Al₂O₃-onto-HfO₂ stacks film has been shown to be a practical high-κ material that can withstand temperatures of up to 800 °C.

2. Experimental

Figure 1 shows the process flow charts of Al₂O₃-onto-HfO₂ stacks, HfO₂-onto-Al₂O₃ stacks and HfO₂ on graphene directly deposited by ALD. After transferring graphene onto SiO₂/Si

and Si substrates (Step 1), four cycles of pre-H₂O treatment were performed prior to dielectric films growth in order to make the graphene surface covered with physically adsorbed H₂O molecules to act as nucleation sites (Step 2). In the pre-H₂O treatment process, the time of graphene exposing to H₂O was adjusted by ALD-cycles rather than prolonging the exposure time at one cycle. One pre-H₂O treatment cycle contained 1 s supply of H₂O and a 10s purge of excess H₂O. If graphene is over exposed to H₂O at one cycle, it is easy to form large H₂O drops due to inter-molecular attraction between H₂O molecules and hydrophobic property of graphene while minor multi-exposure to H₂O will help H₂O molecules overcome the inter-molecular attraction and have a relatively uniform distribution on graphene surface. 4 cycles of pre-H₂O treatment has proved to be optimal for the subsequent high-κ films deposition on graphene and details of pre-H₂O treatment optimization can be found in our previous work.¹⁸ The Al₂O₃-onto-HfO₂ stacks were deposited onto graphene from Hf(NC₂H₅CH₃)₄ (TEMAH), TMA and H₂O by a two-temperature-growth mode. First, 30 ALD cycles of HfO₂ film were deposited onto graphene (Step 3) followed by 15 ALD cycles of Al₂O₃ film (Step 4) at 100 °C. 15 ALD cycles of HfO₂ and Al₂O₃ deposited on Si at 100 °C were both 1 nm, confirmed by SE measurements. Second, Step 3 and Step 4 were repeated twice after the chamber temperature was elevated to 200 °C (Step 5). One ALD cycle consisted of the following four steps: (1) a 1.2s pulse of TEMAH (or TMA) in duration; (2) a 10s purge of excess TEMAH (or TMA) and any byproducts; (3) a 1 s supply of H₂O; (4) a 10s purge of excess H₂O and any byproducts. For the purpose of investigating the effects of dielectrics growth order optimization on the Al₂O₃-doped HfO₂ films property enhancement, another sample with reversed deposition order of HfO₂ and Al₂O₃ (HfO₂-onto-Al₂O₃ stacks) was also deposited on graphene. 15 ALD cycles of Al₂O₃ film was firstly deposited onto graphene followed by 30 ALD cycles of HfO₂ film at 100 °C. Then, this process was repeated twice at 200 °C. For comparison, 135 ALD cycles of pure HfO₂ film was also deposited on graphene (45 ALD cycles of HfO₂ grown at 100 °C and 90 ALD cycles of HfO₂ grown at 200 °C).

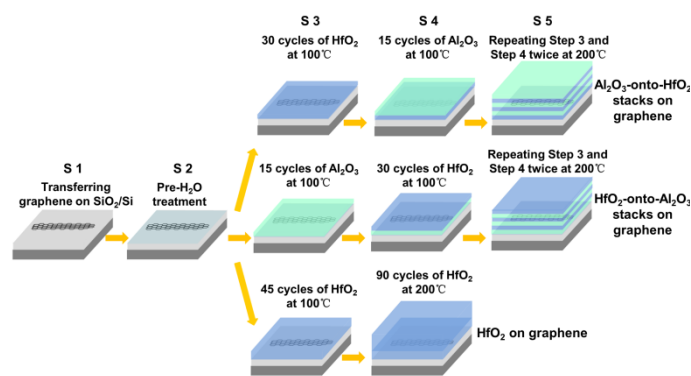
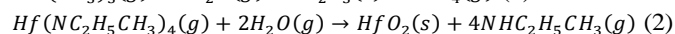
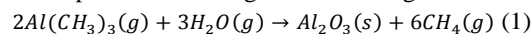


Fig. 1 The process flow charts of Al₂O₃-onto-HfO₂ stacks, HfO₂-onto-Al₂O₃ stacks and HfO₂ deposition on graphene directly by ALD.

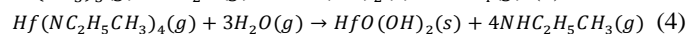
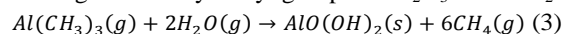
3. Results and discussion

Two temperature regimes were proved to be beneficial for both direct ALD Al₂O₃ and HfO₂ growth on graphene.^{18–20,23} The dielectric film deposited at 100 °C is similar to a seed layer,

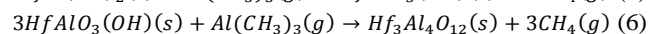
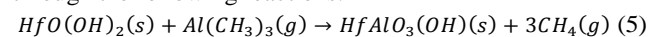
which has a significant effect on the subsequent film deposited at 200 °C.¹³ Besides, there is a huge difference of chemical activity between TEMAH and TMA. Hence, the growth order optimization of HfO₂ and Al₂O₃ plays a vital role in the property enhancement of the integral Al₂O₃-doped HfO₂ films. At the interfacial region of Al₂O₃-onto-HfO₂ or HfO₂-onto-Al₂O₃ stacks, not only did H₂O act as nucleation sites on graphene, but also it could act as an oxidant and react with the metal precursors through the following two reactions:



However, incomplete reactions such as (3) and (4) could occur at the interfacial region due to low growth temperature (100 °C), leading to some hydroxyl groups in Al₂O₃ and HfO₂ films.



This adverse effect on HfO₂ was more serious than Al₂O₃ due to lower chemical activity of TEMAH than TMA. For Al₂O₃-onto-HfO₂ stacks growth, TMA could permeate into beneath HfO₂ matrixes, where pinholes existed due to the relatively large size of TEMAH, and react with hydroxyls in HfO₂ through the following reactions:



These two reactions consumed the hydroxyl groups in HfO₂, promoted Al₂O₃ doping in HfO₂, and enhanced the interfacial region property of Al₂O₃-onto-HfO₂ stacks. Nevertheless, for HfO₂-onto-Al₂O₃ stacks, it was difficult for TEMAH to fill into the interstitial space of Al₂O₃ due to the moderate chemical activity and large molecules size of TEMAH precursor. As a result, there were more hydroxyl groups in the interfacial region of HfO₂-onto-Al₂O₃ stacks than Al₂O₃-onto-HfO₂ stacks. To confirm this inference, XPS was implemented to analyze the element components in the interfacial regions of Al₂O₃-onto-HfO₂ stacks (30 ALD cycles of HfO₂ covered with 15 ALD cycles of Al₂O₃ grown at 100 °C) and HfO₂-onto-Al₂O₃ stacks (15 ALD cycles of Al₂O₃ covered with 30 ALD cycles of HfO₂ grown at 100 °C). All the XPS peaks were calibrated with the C 1s peak located at 284.8 eV. As shown in Figures 2a–d, for both Al₂O₃-onto-HfO₂ and HfO₂-onto-Al₂O₃ stacks, Al 2p peak could be fitted as a symmetric single peak at 74.8 eV; the peak positions of Hf 4f_{5/2} and Hf 4f_{7/2} were at 19.1 eV and 17.5 eV, respectively, and the binding energy difference was 1.6 eV. These results clearly showed the existence of Al³⁺ and Hf⁴⁺ in Al₂O₃-onto-HfO₂ and HfO₂-onto-Al₂O₃ stacks. Deconvolution of O 1s peak revealed three Gaussian–Lorentzian features corresponding to three distinct chemical states. As shown in Figures 2e and 2f, the peak located at 531.4 eV originated from hydroxyl groups.^{24,25} The other two peaks located at 533 eV and 530.5 eV originated from Al–O bonds and Hf–O bonds, respectively.^{26,27} Compared with HfO₂-onto-Al₂O₃ stacks (Figure 2f), the Hf–O bond peak in Al₂O₃-onto-HfO₂ stacks upshifted while the hydroxide bond peak downshifted (Figure 2e), indicating that for Al₂O₃-onto-HfO₂ stacks, TMA could permeate into beneath HfO₂ matrixes, consume hydroxyl groups in HfO₂ and promote Al₂O₃ doping in HfO₂.

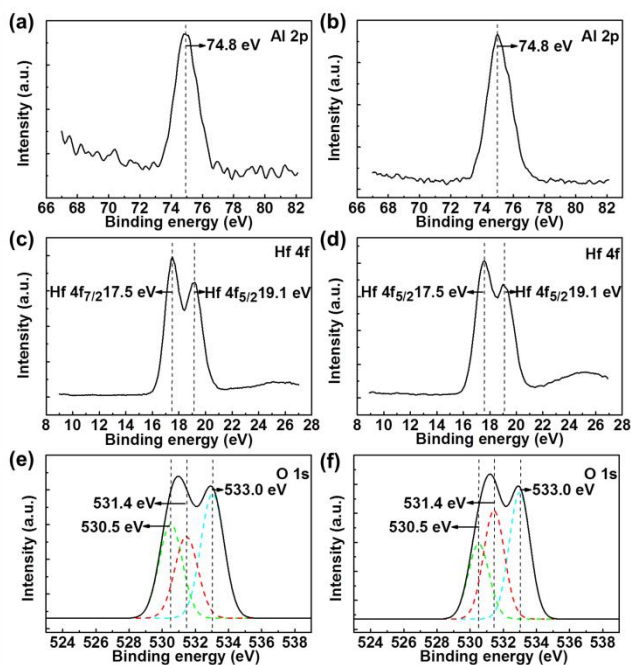


Fig. 2 XPS analysis of Al_2O_3 -onto- HfO_2 stacks on graphene. Al 2p (a), Hf 4f (c) and O1s (e); XPS analysis of HfO_2 -onto- Al_2O_3 stacks on graphene; Al 2p (b), Hf 4f (d) and O1s (f).

AFM was employed to investigate the surface morphology difference of Al_2O_3 -onto- HfO_2 stacks, HfO_2 -onto- Al_2O_3 stacks and HfO_2 deposited directly on graphene under the same ALD growth conditions. Figure 3a-d shows the AFM images of pristine graphene, H_2O -based ALD Al_2O_3 -onto- HfO_2 stacks, HfO_2 -onto- Al_2O_3 stacks and HfO_2 on graphene, respectively. The Al_2O_3 -onto- HfO_2 stacks were pinhole-free and continuously covered the graphene surface with a surface root mean square (RMS) roughness of 0.8 nm, which was comparable to the surface of pristine graphene with a roughness of 0.4 nm. Due to high chemical activity of TMA and micro-molecular property of Al_2O_3 , Al_2O_3 could easily permeate into beneath HfO_2 matrixes, where pinholes existed, and formed continuous and compact Al_2O_3 -doped HfO_2 films. However, for the structure of HfO_2 -onto- Al_2O_3 stacks, as shown in Figure 3c, the surface morphology was loose, pinholes were obvious, and the RMS roughness reached to 1.3 nm. The rough morphology of HfO_2 -onto- Al_2O_3 stacks originated from the moderate chemical activity and large molecules size of TEMAH precursor, where the underneath layer of Al_2O_3 was discontinuous and adhered to graphene tightly; TEMAH could not fill into the interstitial space of Al_2O_3 , and Al_2O_3 upper diffusion into HfO_2 matrix was also suppressed. Therefore, the HfO_2 and Al_2O_3 growth order played a key role in the morphology improvement of Al_2O_3 - HfO_2 stacks film on graphene. As shown in Figure 3d, 9 nm pure HfO_2 did not fully cover the graphene surface and pinholes were serious with a high RMS roughness of 1.2 nm. Although 100°C contributed to the physical absorption of H_2O on graphene,²⁸ it did not conduce to the growth mode transformation for HfO_2 from “island growth” mode to “layer-by-layer growth” mode because

of the lower activity of TEMAH than TMA. Thus, there might be insufficient nucleation sites for subsequent HfO_2 deposition at 200°C , leading to discontinuity and serious pinholes in HfO_2 films. As a consequence, Al_2O_3 -doping is vital to the property enhancement of HfO_2 films directly grown onto graphene by ALD.

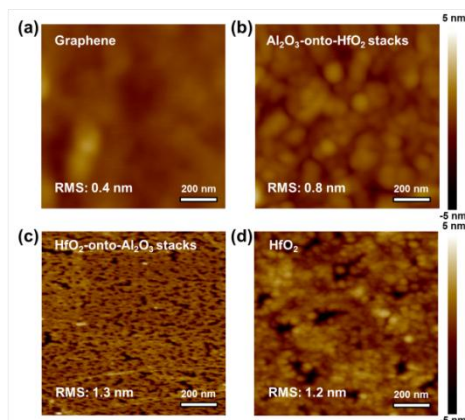


Fig. 3 AFM images of graphene with and without high- κ dielectric films: (a) pristine graphene; (b) Al_2O_3 -onto- HfO_2 stacks on graphene; (c) HfO_2 -onto- Al_2O_3 stacks on graphene; (d) HfO_2 on graphene.

In order to further demonstrate the effects of growth order optimization on the property enhancement of Al_2O_3 -doped HfO_2 films on graphene, GIXRD was carried out to analyze the crystallinity of Al_2O_3 -onto- HfO_2 stacks, HfO_2 -onto- Al_2O_3 stacks and HfO_2 on graphene at the same two-temperature-regime ALD growth mode. The measurement was carried out at the Shanghai Synchrotron Radiation Facility. The X-ray wavelength was 0.124 nm and the X-ray beam was incident at a grazing angle of 0.5° . All three samples were treated by rapid thermal annealing (RTA) at 800°C for 30s before GIXRD measurement. Background contributions were removed from the patterns as shown in Figure 4. Diffraction peaks of HfO_2 and HfO_2 -onto- Al_2O_3 stacks indicated their crystalline phases while the profile of Al_2O_3 -onto- HfO_2 stacks showed no peak, indicating the amorphous nature. The peaks at 19.9° , 22.9° and 25.5° from the HfO_2 profile, shown in Figure 4a, could be assigned to the monoclinic crystal structure, consistent to the knowledge that pure HfO_2 preferred to form the monoclinic structure.²⁹ The GIXRD pattern of HfO_2 -onto- Al_2O_3 stacks exhibited two strong peaks at 30.9° and 35.9° , shown in Figure 4b, while the peak at 22.9° downshifted. In addition, the peak number of HfO_2 -onto- Al_2O_3 stacks reduced, indicating Al_2O_3 -doping could act as a network modifier while the bonding of Al_2O_3 and HfO_2 in HfO_2 -onto- Al_2O_3 stacks was not strong enough to remain the amorphous phase. As shown in Figure 4c, no diffraction peak was detected, manifesting the close bonding of Al_2O_3 and HfO_2 in Al_2O_3 -onto- HfO_2 stacks film and its high maintainable capacity in amorphous state.

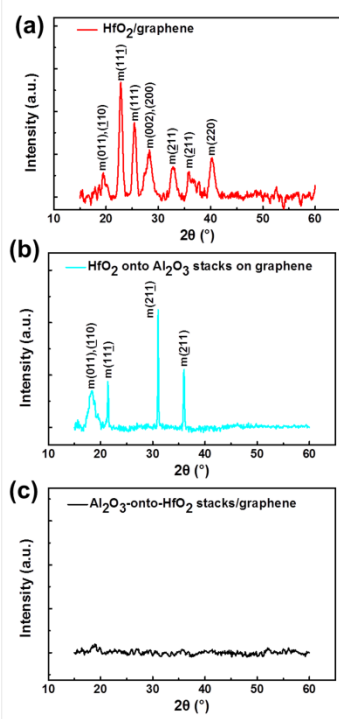


Fig. 4 GIXRD patterns of high- κ dielectric films on graphene: (a) HfO₂ on graphene; (b) HfO₂-onto-Al₂O₃ stacks on graphene; (c) Al₂O₃-onto-HfO₂ stacks on graphene

Besides the AFM and GIXRD measurements, SE was applied for the investigation of optical properties difference between Al₂O₃-onto-HfO₂ stacks, HfO₂-onto-Al₂O₃ stacks and HfO₂ on graphene. The refractive index (n) and the extinction coefficient (k) were directly obtained from the SE results. And the absorption coefficient (α) could be calculated from the extinction coefficient (k) and wavelength (λ) by the following formula:

$$\alpha = 4\pi k / \lambda \quad (1)$$

Both the refractive index and the absorption coefficient were related to the microstructure of the films. As the crystallinity improved, the n value increased,^{30,31} while the change of crystallinity would also disturb the absorption spectra of dielectric films.^{30,32} As shown in Figure 5a, compared to HfO₂ and HfO₂-onto-Al₂O₃ stacks on graphene, an obvious reduction of the refractive index values were detected in the near ultraviolet region (from 250 nm to 400 nm) for Al₂O₃-onto-HfO₂ stacks. All the samples had an absorption edge in the near ultraviolet region, as shown in Figure 5b, while the absorption coefficients of Al₂O₃-onto-HfO₂ stacks on graphene in this region were less than those of HfO₂ and HfO₂-onto-Al₂O₃ stacks on graphene. In addition, the absorption coefficients of Al₂O₃-onto-HfO₂ stacks on graphene slightly upshifted in the visible light region (from 400 nm to 800 nm), compared with HfO₂ and HfO₂-onto-Al₂O₃ stacks on graphene. These phenomena also indicated the crystallinity difference between Al₂O₃-onto-HfO₂ and HfO₂-onto-Al₂O₃ stacks. Al₂O₃ and HfO₂ bonded more closely in Al₂O₃-onto-HfO₂ stacks, leading to higher maintainable capacity in amorphous state of high- κ films on graphene.

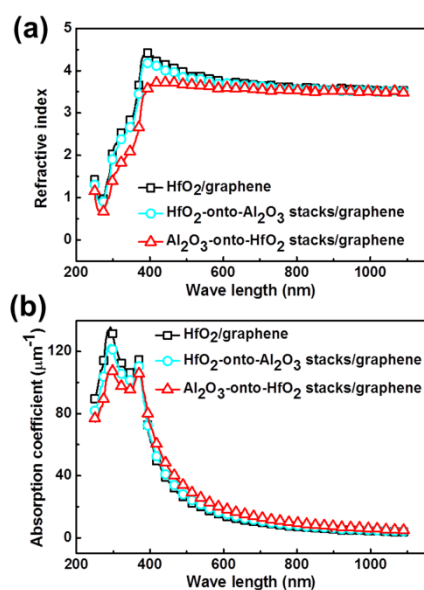


Fig. 5 Optical analysis of Al₂O₃-onto-HfO₂ stacks, HfO₂-onto-Al₂O₃ stacks and HfO₂ on graphene: (a) the refractive indexes of Al₂O₃-onto-HfO₂ stacks, HfO₂-onto-Al₂O₃ stacks and HfO₂ on graphene; (b) the absorption coefficients of Al₂O₃-onto-HfO₂ stacks, HfO₂-onto-Al₂O₃ stacks and HfO₂ on graphene.

HRTEM and C-V measurements were also utilized to verify the high quality of Al₂O₃-onto-HfO₂ stacks on graphene grown by H₂O-based ALD. As shown in Figure 5a, the thicknesses of Al₂O₃-onto-HfO₂ stacks deposited at 100 °C and 200 °C were 3 nm and 6 nm, respectively, obtained from the comparison with the HRTEM scale. Utilizing two-temperature growth mode in the ALD processes is due to two reasons. One is that physically absorbed H₂O on graphene is performed to act as nucleation sites since graphene surface is chemical inert and lacks of dangling bonds. However, at high temperature of 200 °C, the thermal energy gained by H₂O molecules is sufficient to evaporate H₂O molecules from graphene surface, leading to few nucleation sites for the subsequent high- κ films growth. Thus, the chosen initial growth temperature was controlled at 100 °C. Nevertheless, the growing temperature of 100 °C will introduce abundant hydroxyl groups in the high- κ films due to incomplete reaction between TMA (TEMAH) and H₂O, which leads to loose structures (shown in Figure 6a) and low permittivity of high- κ films. Therefore, two-temperature (100/200 °C) was utilized to grow Al₂O₃-onto-HfO₂ stacks on graphene. Although the Al₂O₃-onto-HfO₂ stacks film grown at 100 °C showed a loose structure, it could act as a seed-like layer and supplied sufficient nucleation sites for the following film growth at 200 °C. Sufficient nucleation sites along with high temperature (200 °C) benefited the property enhancement of Al₂O₃-onto-HfO₂ stacks, leading to continuous and uniform dielectrics (shown in Figure 6a). Al₂O₃-doping also contributed to the compactness of Al₂O₃-onto-HfO₂ stacks. Due to the micro-molecular property of Al₂O₃ and high activity of TMA, Al₂O₃ was intelligent to fill the pinholes of HfO₂ and formed a compact high- κ film during the ALD process. Both of the

Al₂O₃-onto-HfO₂ stacks deposited at 100 °C and 200 °C exhibited an amorphous microstructure, which were also confirmed by GIXRD analysis. Electrical analysis was performed by an Agilent B1505A semiconductor parameter analyzer. The metal-oxide-graphene (MOG) structure, as shown in Figure 6b, was explored for the C-V measurements and the series model was utilized.³³ The Au (100 nm)/Ti (10 nm) electrodes were fabricated through a shadow mask sputtering. The area of each circular electrode was 0.01 mm² and the distance between two electrodes was 0.8 mm. The actual capacitance value was double of the measured one due to the series connection of two same capacitors. In addition, the dual-frequency method was introduced to extract the capacitance according to the following formula:

$$C = (f_1^2 C_1 - f_2^2 C_2) / (f_1^2 - f_2^2) \quad (2)$$

where C_1 and C_2 referred to the values measured at the frequency of f_1 and f_2 , respectively.^{18,20,34} C-V measurements were implemented at two different frequencies (200 kHz and 500 kHz) and extracted by equation (2) as shown in Figure 4b. All the C-V curves showed the expected broad V-shape due to the quantum capacitance (C_Q) of graphene.^{35,36} C_Q was in series to the oxide capacitance (C_{ox}) and C_{ox} was approximately an order of magnitude lower than C_Q at the bias away from the Dirac Point of graphene. Thus, the measured capacitance at ± 2 V was close to C_{ox} , and the capacitance of Al₂O₃-onto-HfO₂ stacks on graphene was 1.18 $\mu\text{F}/\text{cm}^2$. The relative permittivity and EOT of Al₂O₃-onto-HfO₂ stacks were 12 and 2.9 nm, respectively, according to equation (3) and (4).

$$\varepsilon = C_{ox} t_{ox} / (\varepsilon_0 A) \quad (3)$$

$$EOT = \varepsilon_0 \varepsilon_{SiO_2} A / C_{ox} \quad (4)$$

where A was the electrode area, ε_0 was the vacuum dielectric constant and t_{ox} was the thickness of Al₂O₃-onto-HfO₂ stacks. The relative permittivity of Al₂O₃-onto-HfO₂ stacks was a little smaller than the one of pure HfO₂ (15-25) due to Al₂O₃-doping. However, the permeation of Al₂O₃ into HfO₂ was beneficial for the surface morphology smoothness, microstructure compactness and amorphous state stability of the integrate high- κ films.

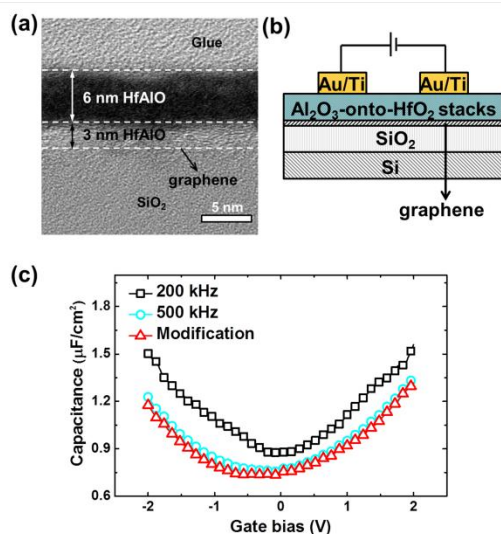


Fig. 6 (a) The HRTEM image of Al₂O₃-onto-HfO₂ stacks on graphene. (b) The schematic MOG structure for C-V measurements. (c) C-V measurements of Al₂O₃-onto-HfO₂ stacks on graphene performed at different frequencies: 200 kHz, 500 kHz, and extracted by dual-frequency method.

It was worth mentioning that uniform intermixing of Al₂O₃ and HfO₂ was obtained in our work. This conjecture was firstly supported by the fact that no layered structures were observed by HRTEM (Figure 6a). Furthermore, there was a huge difference of per-unit-length capacitance between Al₂O₃-onto-HfO₂ stacks film and the one of segregated Al₂O₃ and HfO₂. The per-unit-length capacitances of pure ALD Al₂O₃ and HfO₂ on graphene were 0.7 $\mu\text{F}/\text{cm}^2$ and 2.7 $\mu\text{F}/\text{cm}^2$, respectively,^{18,19} and the calculated per-unit-length capacitance of high- κ film with segregated Al₂O₃ (3 nm) and HfO₂ (6 nm) was 0.21 $\mu\text{F}/\text{cm}^2$, which was much less than the one of Al₂O₃-onto-HfO₂ stacks film (1.18 $\mu\text{F}/\text{cm}^2$). The high per-unit-length capacitance of Al₂O₃-onto-HfO₂ stacks was due to incorporation of Al₂O₃ into HfO₂ and this result agreed well with M. Cho et al.'s and C. An et al.'s reports.^{37,38} Finally, the well-known porous structure of 9 nm thick HfO₂¹⁹ and the high diffusivity of TMA along the HfO₂ surface supported the feasibility of near uniform mixing of the resulting multi-layered stacks of Al₂O₃-HfO₂. We thus proposed that the Al₂O₃-onto-HfO₂ stacks fabricated using the approach described in this paper was effectively Al₂O₃-HfO₂ alloy. In addition, because of the much smaller amount of Al₂O₃ relative to HfO₂ employed, the resulting film could be viewed as Al₂O₃-doped HfO₂.

Raman spectra were performed to determine whether H₂O-based ALD introduced any defects or disorder into graphene. As illustrated in Figure 7a, the pristine graphene had a weak D band peak at 1350 cm⁻¹, a G band peak at 1586 cm⁻¹, and a sharp 2D band peak at 2680 cm⁻¹. The weak D band peak might be due to a little wrinkle generated during the transferring process. The full width at half maximum (FWHM) of 2D band was 40 cm⁻¹ and the I_{2D}/I_G ratio was greater than 1.25, which both indicated that the graphene sample was monolayer. After ALD Al₂O₃-onto-HfO₂ stacks growth, no raise of defect-related D band was detected (shown in Figure 7b), implying that no defects or disorder were introduced into the sp² hybridized carbon structure of graphene by the H₂O-based ALD process.

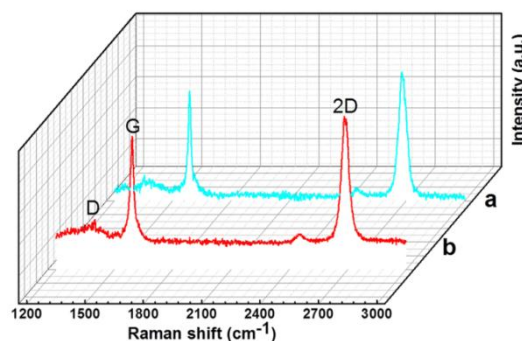


Fig. 7 Raman spectra of graphene with and without Al₂O₃-onto-HfO₂ stacks: (a) pristine graphene; (b) graphene with Al₂O₃-onto-HfO₂ stacks

4. Conclusions

In summary, we have directly deposited Al₂O₃-doped HfO₂ films on graphene by H₂O-based ALD without any seeded layer or functionalization. Moreover, the growing order of Al₂O₃ and HfO₂ was certificated to affect the properties of the integrate high- κ films. The structure of Al₂O₃-onto-HfO₂ stacks was beneficial for the doping of Al₂O₃ into HfO₂ matrixes more than HfO₂-onto-Al₂O₃ stacks did due to the micro-molecular property of Al₂O₃ and high chemical activity of TMA. Al₂O₃-doping could act as a network modifier and maintain the amorphous structure of Al₂O₃-onto-HfO₂ stacks on graphene. The surface RMS of Al₂O₃-onto-HfO₂ stacks film was down to 0.8 nm and its capacitance was up to 1.18 $\mu\text{F}/\text{cm}^2$, indicating high quality of Al₂O₃-doped HfO₂ films on graphene. The relative permittivity and the EOT of Al₂O₃-onto-HfO₂ stacks film were 12 and 2.9 nm, respectively. Moreover, the growth process of Al₂O₃-onto-HfO₂ stacks film introduced no defects into graphene. We believe this technique is very promising for fabrications of novel graphene-based devices

Acknowledgements

This work is funded by the National Natural Science Foundation of China (Grant No. 11175229). The authors would like to thank Prof. Zengfeng Di, Dr. Xiaohu Zheng and Dr. Haoran Zhang for technical assistance and discussions. The authors also thank the staff of beam line BL14B1 in Shanghai Synchrotron Radiation Facility for GIXRD measurements.

Notes and references

^a State Key Laboratory of Functional Materials for Informatics, Institute of Microsystem and Information Technology, Chinese Academy of Sciences, Changning Road 865, Shanghai 200050, P. R. China.

*E-mail: xh_cheng@mail.sim.ac.cn

^b Department of Materials Science and Engineering, University of California Los Angeles, California 90095, USA.

^c Shanghai Synchrotron Radiation Facility, Zhangheng Road 239, Shanghai 200061, P. R. China.

- 1 K. S. Novoselov, A. K. Geim, S. V. Morozov, D. Jiang, Y. Zhang, S. V. Dobonos, I. V. Grigorieva and A. A. Firsov, *Science*, 2004, **306**, 666-669.
- 2 A. A. Balandin, S. Ghosh, W. Bao, I. Calizo, D. Teweldebrhan, F. Miao and C. N. Lau, *Nano Lett.*, 2008, **8**, 902-907.
- 3 K. I. Nolotin, K. J. Sikes, Z. Jiang, M. Klima, G. Fudenberg, J. Hone, P. Kim and H. L. Stormer, *Solid State Commun.*, 2008, **146**, 351-355.
- 4 M. D. Stoller, S. Park, Y. Zhu, J. An and R. S. Ruoff, *Nano Lett.* 2008, **8**, 3498-3502.
- 5 S. H. Chae, W. J. Yu, J. J. Bae, D. L. Duong, D. Perello, H. Y. Jeong, Q. H. Ta, T. H. Ly, Q. A. Vu and M. Yun, *Nat. Mater.* 2013, **12**, 403-409.
- 6 R. Addou, A. Dahal and M. Batzill. *Nat. Nanotechnol.*, 2013, **8**, 41-45.
- 7 D. B. Farmer, H. Chiu, Y. Lin, K. A. Jenkins, F. Xia and P. Avouris. *Nano Lett.*, 2009, **9**, 4474-4478.
- 8 X. Hong, A. Posadas, K. Zou, C. H. Ahn and J. Zhu. *Phys. Rev. Lett.*, 2009, **102**, 136808
- 9 W. Mehr, J. Dabrowski, J. C. Scheytt, G. Lippert, Y. Xie, M. C. Lemme, M. Ostling and G. Lupina. *IEEE Electr. Device L.*, 2012, **33**, 691-693.
- 10 V. K. Sangwan, D. Jariwala, S. A. Filippone, H. J. Karmel, J. E. Johns, J. M. P. Alaboson, T. J. Marks, L. J. Lauhon and M. C. Hersam. *Nano Lett.*, 2013, **13**, 1162-1167.
- 11 K. Zou, X. Hong, D. Keefer and J. Zhu, *Phys. Rev. Lett.*, 2010, **105**, 126601.
- 12 L. Wang, J. J. Travis, A. S. Cavanagh, X. Liu, S. P. Koenig, P. Y. Huang, S.M. George and J.S. Bunch, *Nano Lett.*, 2012, **12**, 3706-3710.
- 13 W. C. Shin, T. Y. Kim, O. Sul and B. J. Cho, *Appl. Phys. Lett.*, 2012, **101**, 033507.
- 14 B. K. Lee, S. Y. Park, H. C. Kim, K. Cho, E. M. Vogel, M. J. Kim, R. M. Wallace and J. Kim, *Appl. Phys. Lett.*, 2008, **92**, 203102.
- 15 D. B. Farmer, Y. Lin, A. Afzali-Ardakani and P. Avouris, *Appl. Phys. Lett.*, 2009, **21**, 213106.
- 16 S. Kim, J. Nah, I. Jo, D. Shahrjerdi, L. Colombo, Z. Yao, E. Tutuc and S. K. Banerjee, *Appl. Phys. Lett.*, 2009, **94**, 062107.
- 17 M. J. Hollander, M. LaBella, Z. R. Hughes, M. Zhu, K. A. Trumbull, R. Cavalero, D. W. Snyder, X. Wang, E. Hwang, S. Datta and J. A. Robinson, *Nano Lett.*, 2011, **11**, 3601-3607.
- 18 L. Zheng, X. Cheng, D. Cao, G. Wang, Z. Wang, D. Xu, C. Xia, L. Shen, Y. Yu and D. Shen, *ACS Appl. Mater. Interfaces*, 2014, **6**, 7014-7019.
- 19 L. Zheng, X. Cheng, D. Cao, Z. Wang, D. Xu, C. Xia, L. Shen and Y. Yu, *J. Vac. Sci. A*, 2014, **32**, 01A103.
- 20 L. Zheng, X. Cheng, D. Cao, Z. Wang, C. Xia and Y. Yu, *Appl. Phys. Lett.*, 2014, **104**, 023112.
- 21 J. Robertson, *J. Appl. Phys.*, 2008, **104**, 124111.
- 22 D. Vanderbilt, X. Zhao and D. Ceresoli, *Thin Solid Films*, 2005, **486**, 125-128.
- 23 H. Alles, J. Aarik, A. Aidla, A. Fay, J. Kozlova, A. Niilisk, M. Pärss, M. Rähn, M. Wiesner, P. Hakonen and V. Sammelselg. *Cent. Eur. J. Phys.*, 2011, **9**, 319-324.
- 24 O. Renault, L. G. Gosset, D. Rouchon and A. Ermolieff. *J. Vac. Sci. Technol. A*, 2002, **20**, 1867-1876.
- 25 H. K. Jeong, J. P. Tae, K. K. Seong, C. Deok-Yong, J. Hyung-Suk, Y. L. Sang and S. H. Cheol. *Appl. Surf. Sci.*, 2014, **292**, 852-856.
- 26 C. Deok-Yong, S. J. Hyung, Y. Il-Hyuk, H. Y. Jung, K. K. Hyo, Y. L. Sang, H. J. Sang, H. Seungwu, H. K. Jeong, J. P. Tae, P. Byeong-Gyu and S. H. Cheol. *Chem. Mater.*, 2012, **24**, 3534-3543.
- 27 J. van den Brand, P. C. Snijders, W. G. Sloof, H. Terryn and J. H. W. de Wit. *J. Phys. Chem. B*, 2004, **108**, 6017-6024.
- 28 J. Qu, Physical Chemistry, China Renmin University Press: Beijing, China, 2009.
- 29 D. Cho, T. J. Park, K. D. Na, J. H. Kim and C. S. Hwang, *Phys. Rev. B: Condens. Matter Mater. Phys.*, 2008, **78**, 132102.
- 30 A. A. Chaaya, R. Viter, I. Baleviciute, M. Bechelany, A. Ramanavicius, Z. Gertner, D. Erts, V. Smyntyna and P. Miele, *J. Phys. Chem. C*, 2014, **118**, 3811-3819.
- 31 Y. E. Hong, Y. S. Kim, K. Do, D. Lee, D. H. Ko, J. H. Ku and H. Kim, *J. Vac. Sci. A*, 2005, **23**, 1413-1418.

Journal Name

- 32 J. Aarik, H. Mandar, M. Kirm and L. Pung, *Thin Solid Films*, 2004, **466**, 41-47.
- 33 K. J. Yang and C. Hu, *IEEE Trans. Electron Devices*, 1999, **46**, 1500-1501.
- 34 Z. Luo and T. P. Ma, *IEEE Electr. Device L.*, 2004, **25**, 655-657.
- 35 T. Fang, A. Konar, H. Xing and D. Jena, *Appl. Phys. Lett.*, 2007, **91**, 092109.
- 36 J. Xia, F. Chen, J. Li and N. Tao, *Nat. Nanotechnol.*, 2009, **4**, 505-509.
- 37 M. Cho, H. S. Chang, Y. J. Cho, D. W. Moon, K. Min, R. Sinclair, S. K. Kang, D. Ko, J. H. Lee, J. H. Gu and N. I. Lee, *Appl. Phys. Lett.*, 2004, **84**, 571.
- 38 C. An, C. Mahata, Y. Byun and H. Kim, *J. Phys. D: Appl. Phys.*, 2013, **46**, 275301.